Stress evaluation of a guillotine cutter with steels of varying yield strength and thickness using displacement and snap signals

Juhani Nissilä *

* *Control Engineering Research Group, Faculty of Technology P.O.Box 4300, FI-90014 University of Oulu, Finland (e-mail: juhani.nissila@oulu.fi)*

Abstract: Ultra high-strength steels are becoming more common in the steel industry. The mechanical cutting of these steels with guillotine cutters is desirable when compared to plasma or laser cutters, but it is not clear how much more stress these ultra high-strength steels can cause to the guillotine cutter. The purpose of this paper is to analyse thousands of cutting events of steels of varying yield strength and thickness from a guillotine cutter and plot informative norms from these events. These norms are generalised l_p norms of displacement and its fourth derivative, snap. According to the findings, at least for moderately thin (5 - 10 mm) ultra high-strength steels (yield strengths 900 - 1100 MPa) the stress on the cutter is not much higher than for softer conventional thin steels. Slower operating speed has also reduced stress levels considerably when cutting ultra high-strength steels with yield strengths up to 1330 MPa. The acceleration measurements are from SSAB Europe Oy in Finland.

Keywords: Stress evaluation, steel cutter, ultra high-strength steels, generalised l_p norms, fractional derivatives, snap, MIT indices,

1. INTRODUCTION

The aim of this paper is to utilise vast data of acceleration measurements of steel cutting events from a guillotine cutter. Based on a previous study (Karioja and Lahdelma, 2015), displacement and snap signals are used to calculate high-order norms and these two values for each cutting event are plotted in order to see what kinds of 2D distributions steels of different strength and thickness form. From these distributions, the stress on the cutter components can be estimated.

2. SIGNAL PROCESSING

2.1 Fractional derivatives and integrals

Although only integer order derivatives and integrals are used in the numerical work of this paper, the general theory for fractional derivatives and integrals is presented here briefly since the numerical algorithm works for any order $z \in \mathbb{C}$.

Fractional calculus is a branch of mathematical analysis which studies the concept of generalising the concepts of differentiation and integration to an arbitrary real or even complex order. These generalisations are not unique and generally depend on the choice of the lower limit of integration and the order of differential and integral operators. The definition most suitable for mechanical vibration utilises the *Fourier transform* $X(\nu)$ of the signal $x(t)$

$$\mathcal{F}\{x(t)\} = X(\nu) = \int_{-\infty}^{\infty} x(t) e^{-i2\pi\nu t}\,\mathrm{d}t. \tag{1}$$

Its *inverse transform* is defined as

$$\mathcal{F}^{-1}\{X(\nu)\} = \int_{-\infty}^{\infty} X(\nu) e^{i2\pi\nu t}\,\mathrm{d}\nu. \tag{2}$$

If t is time in seconds (s), then the variable ν of the transformed function is frequency in hertz (Hz).

Let $z = \alpha + i\beta \in \mathbb{C}$ and X is the Fourier transform of x. The *differintegral* of order z is

$$\begin{aligned} x^{(z)}(t) &= \mathcal{F}^{-1}\big\{(i2\pi\nu)^z X(\nu)\big\} \\ &= \int_{-\infty}^{\infty} (i2\pi\nu)^z X(\nu)\, e^{i2\pi\nu t}\,\mathrm{d}\nu, \end{aligned} \tag{3}$$

where $(i2\pi\nu)^z = e^{z\ln(2\pi|\nu|)+iz\frac{\pi}{2}\mathrm{sign}(\nu)}$ is the principal value of the exponential function for the general complex z. For real z, there is no need to consider such choices.

These ideas were first presented by Fourier for real order differintegrals in (Fourier, 1822). A closely related definition for periodic signals was introduced by Hermann Weyl using the Fourier series (Weyl, 1917). Both of these definitions correspond to the more well known Riemann-Liouville fractional integral and derivative with lower limit $-\infty$ (Samko et al., 1993). This is informative, since it means that in the Fourier definition there is no built-in moment of time when the vibration amplitude must be zero.

In practice, we only have a sampled sequence $\mathbf{x} = (x_0, \ldots, x_{N-1})$ of length $T = \Delta t \cdot N$, where Δt is the

sampling interval, and we can thus approximate the signal's Fourier transform with the *Discrete Fourier transform* (DFT)

$$\mathcal{F}\{x_n\} = X_k = \frac{1}{N}\sum_{n=0}^{N-1} x_n e^{-i2\pi kn/N}. \tag{4}$$

Its *inverse transform* (IDFT) is

$$\mathcal{F}^{-1}\{X_k\} = x_n = \sum_{k=0}^{N-1} X_k e^{i2\pi kn/N}. \tag{5}$$

DFT is better than a mere approximation in the sense that IDFT always returns the original signal values at the sample points. The author has presented an algorithm to calculate the smoothest discrete approximation of the differintegral $x^{(z)}(t)$ in the frequency domain in (Nissilä et al., 2014). The algorithm consists of calculating the DFT coefficients X_k and then forming a new sequence G_k, $0 \le k \le N$-1, with $G_0 = 0$ and

$$\begin{aligned} G_k &= \left(\frac{2\pi ki}{T}\right)^z X_k, && 0 < k < N/2 \\ G_{N+k} &= \left(\frac{2\pi ki}{T}\right)^z X_{N+k}, && -N/2 < k < 0 \\ G_{N/2} &= \left(\frac{\pi N}{T}\right)^z \cos\left(z\frac{\pi}{2}\right) X_{N/2} && \text{(if } N \text{ is even)}. \end{aligned} \tag{6}$$

Finally the differintegrated sequence $x_n^{(z)}$ is calculated with the IDFT

$$x_n^{(z)} = \mathcal{F}^{-1}\{G_k\}. \tag{7}$$

Before calculating the DFT, it is practical to window the signal. This is because DFT assumes the signal to be periodic and thus its endpoints may cause discontinuities in the periodic continuation. The window function utilised in this study was introduced in the article (Lahdelma and Kotila, 2005)

$$w(t) = \begin{cases} 0, & \text{if } t \le 0 \\ \dfrac{1}{A}\displaystyle\int_0^t e^{\left(\tau(\tau - T/\epsilon)\right)^{-1}} \mathrm{d}\tau, & \text{if } 0 < t < T/\epsilon \\ 1, & \text{if } T/\epsilon \le t \le T/2 \\ w(T-t), & \text{if } t > T/2, \end{cases} \tag{8}$$

where $A = \int_0^{T/\epsilon} e^{\left(\tau(\tau - T/\epsilon)\right)^{-1}} \mathrm{d}\tau$ and ϵ is the portion of T for ascent and descent. Function w is infinitely differentiable and, therefore, it preserves the continuity properties of the original signal.

2.2 l_p norms and MIT indices

The *generalised* l_p norm or *Hölder mean* of a differintegrated vector $\mathbf{x}^{(z)}$ is defined by

$$\left\|\mathbf{x}^{(z)}\right\|_{p,\frac{1}{N}} = \left(\frac{1}{N}\sum_{n=1}^{N}\left|x_n^{(z)}\right|^p\right)^{1/p}, \tag{9}$$

for $p \ge 1$. This norm is recognised as the traditional l_p norm with equal weights $1/N$. It is possible to generalise (Bullen, 2003) the concept to $-\infty \le p \le \infty$ by defining the limiting values correctly with

$$\left\|\mathbf{x}^{(z)}\right\|_{p,\frac{1}{N}} = \begin{cases} \left(\displaystyle\sum_{n=1}^{N}\frac{1}{N}\left|x_n^{(z)}\right|^p\right)^{1/p} & \text{if } p \in \mathbb{R}\backslash\{0\} \\ \left(\displaystyle\prod_{n=1}^{N}\left|x_n^{(z)}\right|\right)^{1/N} & \text{if } p = 0 \\ \max\limits_{n=1,\ldots,N}\left|x_n^{(z)}\right| & \text{if } p = \infty \\ \min\limits_{n=1,\ldots,N}\left|x_n^{(z)}\right| & \text{if } p = -\infty. \end{cases} \tag{10}$$

From this we see that the Hölder mean includes many traditional signal features, such as *minimum value* $p = -\infty$, *harmonic mean* $p = -1$, *geometric mean* $p = 0$, *arithmetic mean* $p = 1$, *root mean square* (rms) $p = 2$ and *maximum value* $p = \infty$.

The *MIT index* was first presented in (Lahdelma, 1992) utilising the rms values of integer order derivatives and integrals. Later it has been generalised to real order differintegrals (Lahdelma and Juuso, 2011) and is thus formulated as

$${}^{\tau}MIT^{p_1,p_2,\ldots,p_n}_{\alpha_1,\alpha_2,\ldots,\alpha_n} = \frac{1}{n}\sum_{k=1}^{n} b_{\alpha_k}\frac{\left\|\mathbf{x}^{(\alpha_k)}\right\|_{p_k}}{\left\|\mathbf{r}^{(\alpha_k)}\right\|_{p_k}}, \tag{11}$$

where $\sum_{k=1}^{n} b_{\alpha_k} = 1$, τ is signal length and the signal $\mathbf{r}$ is a reference signal from the machine in good condition. Typically MIT increases with decreasing machine condition. The MIT index can also be used to compare stress levels of different operating conditions.

3. VIBRATION MEASUREMENTS

The accelerometer utilised in this study was stud-mounted axially on the bearing housing of the guillotine cutter's worm gear. The worm gear drives a crankshaft which is connected by rods to a beam that holds the upper blade. The cutter mechanism and vibration measurements are described in more detail in (Karioja and Lahdelma, 2015). The sampling frequency is 25.6 kHz and file length is 7 s.

Figures 1, 2, 3, and 4 show the cutting events of 8 mm thick steels with approximate yield strengths 300, 800, 1000, and 1300 MPa respectively. In the first three cases, the cut takes place approximately between 1 - 3 seconds. In the fourth case, the cut begins not until after 5 seconds and this is the case with most ultra high-strength steel cutting events. It was verified from SSAB Europe Oy that the cutter is driven more slowly in this case, which explains the delayed cut and the lower base level of the signal around the cut. The speed is only 30% of the speed that is used with softer steels. The obvious conclusion from these figures is that cutting higher strength steel causes more rapid shock-like vibration.

Figures 5 and 6 show cutting events from 400 MPa and 40 mm and 800 MPa and 16 mm steels, respectively. We see how thickness increases the cutting time. Both of these particular cutting events have sharp peaks at the end or beginning of the cut. This particular phenomenon occurs most often with steels of medium thickness, as we will see from the 2D distributions. At the very end of Figure 5, we see vibrations caused occasionally by a rammer that pushes scrap pieces to a conveyor.

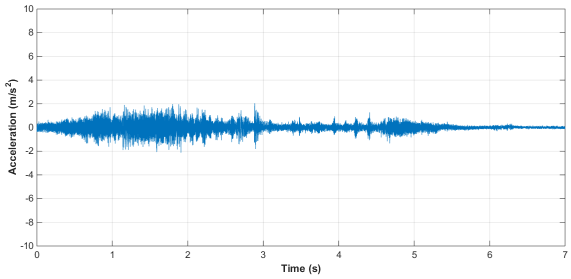

Fig. 1. Acceleration signal when cutting 8 mm thick steel with yield strength 300 MPa.

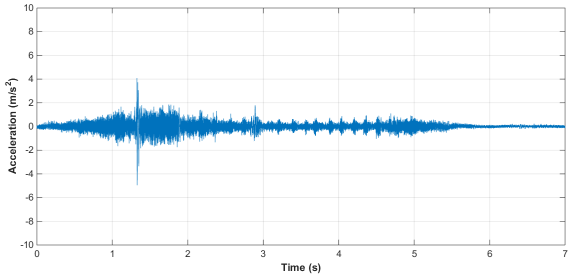

Fig. 2. Acceleration signal when cutting 8 mm thick steel with yield strength 800 MPa.

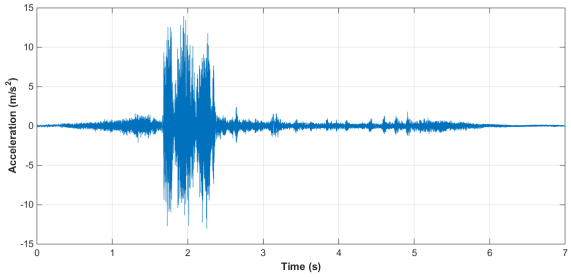

Fig. 3. Acceleration signal when cutting 8 mm thick steel with yield strength 1000 MPa.

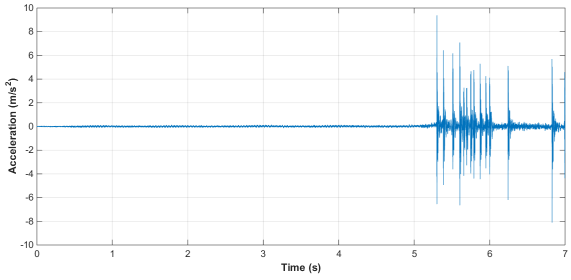

Fig. 4. Acceleration signal when cutting 8 mm thick steel with yield strength 1300 MPa.

4. 2D DISTRIBUTIONS FROM GENERALISED NORMS

In the previous study (Karioja and Lahdelma, 2015) it was observed that cutting events from ultra high-strength steels (probably about 900 MPa) produced higher norm values when the signal was first differentiated. Another observation was that the thickness of the steel was directly proportional to the norm values of the displacement signal,

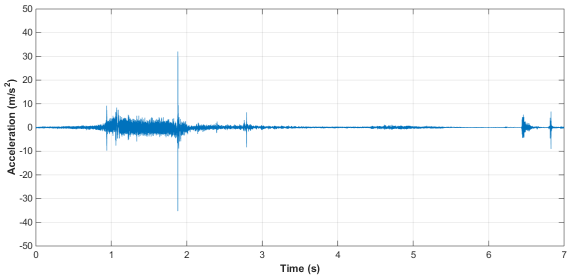

Fig. 5. Acceleration signal when cutting 40 mm thick steel with yield strength 400 MPa.

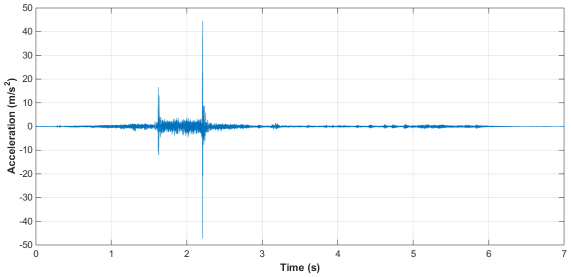

Fig. 6. Acceleration signal when cutting 16 mm thick steel with yield strength 800 MPa.

which can be calculated by numerically integrating twice the measured acceleration signal. Relatively high orders of norm were also observed to be beneficial in both the cases when trying to highlight differences between steels of varying thickness and strength. These results were obtained by calculating real order derivatives and generalised norms with varying α and p and then calculating MIT indices. The signals from cutting events of conventional low strength and thin steel were used as the reference signals. The norms $||\mathbf{x}^{(4)}||_{6,1/N}$ and $||\mathbf{x}||_{8,1/N}$ were selected for further numerical work to analyse the stress caused to the cutter.

The data used in (Karioja and Lahdelma, 2015) consisted only of a handful of cutting events. Also since that study, even higher strength steels are now being cut (up to 1330 MPa) with the same guillotine cutter, although only very thin ones. The aim of this study is to look at the distribution of all the cutting events recorded and visualise them informatively. The visualisation should tell something about the stress on the cutter caused by different steels and also about the amount of variation of cutting events within each steel type. This is why I also chose the same norms $||\mathbf{x}^{(4)}||_{6,1/N}$ and $||\mathbf{x}||_{8,1/N}$ for this numerical work. The second derivative of acceleration, sometimes also known as "snap" or "jounce", has a physical meaning as the acceleration of acceleration and is thus related to rapid changes in the cutting process. The physical meaning of displacement is even more obvious as it shows the movement of the measurement point during the cut. All the calculations were performed using Matlab.

There are 10273 cutting events in total. Of these, 722 have yield strength between 1200 - 1330 MPa. The whole length of the signal was used in the calculations, although it was first windowed with (8) using $\epsilon = 28$. Then the DFT of the signal was calculated and it was filtered with an

ideal filter to the frequency band 5 Hz - 10 kHz. Next, differentiation and integration were carried out in the frequency domain with (6) and the signal was transformed back to the time domain with (7) after which $2 \cdot (7/\epsilon)\,\mathrm{s} = 0.5\,\mathrm{s}$ were rejected from both ends of the signal. Since we are mainly interested in the actual cutting event, a simple algorithm was used to search a two-second part of the remaining signal which very probably corresponds to the cut. First the remaining 6 s was divided into partly overlapping sections with a step of 0.25 s. The 2 s section with the maximum of $||\mathbf{x}^{(4)}||_{1,1/N}$ was selected as the cut. Here $N = 25.6\,\mathrm{kHz} \cdot 2\,\mathrm{s} = 51200$. This norm was chosen for the task, because the snap signal seems to amplify the cut even with conventional soft steels. The low order of norm was selected, since high order could wrongly classify the pushing of the scrap piece to a conveyor, which we see at the end of Figure 5, as the cut. Figure 7 shows how many cutting events were identified with each section. The identified 2 seconds were used to calculate norms $||\mathbf{x}^{(4)}||_{6,1/N}$ and $||\mathbf{x}||_{8,1/N}$ for each signal. 539 cuts occur at the very end of the measurement. These are the ones with yield strengths between 1200 - 1330 MPa. This means that 183 of these 722 ultra high-strength cutting events are not found here. Most of these 183 events actually lack the cut entirely, which has happened probably due to the slower speed of the cutter. Our algorithm has placed the cut for these events quite randomly and calculated norm values that are pretty much zero.

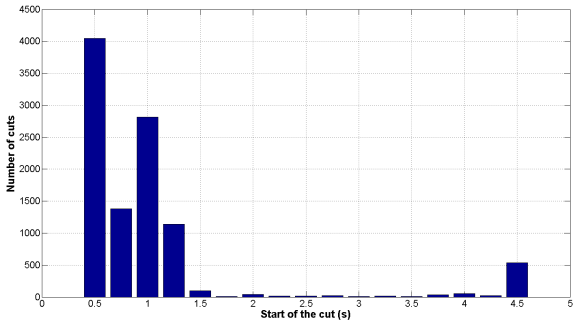

Fig. 7. Distribution of the beginning of the cuts

Figures 8, 9, 12, 13, and 14 all show the same features $||\mathbf{x}^{(4)}||_{6,1/N}$ in the y-axis and $||\mathbf{x}||_{8,1/N}$ in the x-axis for all the cutting events, but the values are coloured according to different types of process information that are in order thickness, yield strength, width, blade clearance, and cut count after blade replacement. Figures 10 and 11 show a close-up of the cases thickness and yield strength. Numerical values for blade clearance and cut count have been omitted, so the colors in Figures 13 and 14 reveal only relative information.

Immediately we see from Figures 8 and 10 that $||\mathbf{x}||_{8,1/N}$ values increase linearly with increasing steel thickness. This is an expected outcome, as the blade has to cut through more material. Another expected result is that the blade clearance in Figure 13 correlates quite perfectly with the colors of Figure 8, since the clearance is automatically set based on steel thickness.

Figures 12 and 14 both have their colors quite uniformly distributed. This indicates that the width of the steel has little influence on the measured vibrations. Most of the steels that were cut in this study were more than 2.5 m wide. The cut count after blade replacement is somehow related to the wear on the blades and is actually used to evaluate the time to change them. The features calculated do not correlate with the cut count, but this does not mean that vibration measurements can not be used to monitor the condition of the cutter blades, since the true condition of the blades is unknown.

From Figures 9 and 11 we see that steels of different strength form various patterns. Most notable is the tight group of steels with yield strengths 900 - 1100 MPa and thicknesses 5 - 10 mm (based on observing the same group from Fig. 10). These steels have in general higher $||\mathbf{x}^{(4)}||_{6,1/N}$ values than the softer steels of the same thickness and also less variation.

Another interesting group is formed by the ultra high-strength steels (1200 - 1330 MPa) that we noticed to have peculiar vibration signals in Fig. 4. These are mostly located on the lower left corner in Fig. 11. The ones whose norms are almost zero are probably either cancelled cuts or the timing of the cut has gone completely wrong and thus the recording is entirely noise or empty running of the cutter. The cuts recorded still in general have lower $||\mathbf{x}^{(4)}||_{6,1/N}$ values than the steels of strength 900 - 1100 MPa. So although these higher strength steels cause rapid-shock like vibration, the overall vibration levels are not very high and do not cause significant values of norms.

An interesting observation from Figures 8 and 9 is also that the highest $||\mathbf{x}^{(4)}||_{6,1/N}$ values typically belong to steels of thickness 20 - 35 mm and yield strengths 300 - 1000 MPa. Examples of these cases are shown in Figures 5 and 6. This phenomenon was observed in (Karioja and Lahdelma, 2015) as well, where the *MIT* indices calculated using those norms where higher for soft steels of thickness 20 mm than for 30 mm. There is no sure explanation for this. One possibility is that the blade clearance does not match perfectly the steel thickness in the mid-range and thus sometimes causes extra shocks in the cut. Another possibility is that the steels in this class may have a lot of variation in their material properties.

5. CONCLUSIONS

The calculations from the vibration measurements of the cutting events have shown that $||\mathbf{x}||_{8,1/N}$ values increase linearly with increasing steel thickness. Values $||\mathbf{x}^{(4)}||_{6,1/N}$ on the other hand are generally higher with ultra high-strength steels (900 - 1100 MPa) in the case of thin material, but we do not see such separation with thicker steels. The ultra high-strength steels with yield strengths between 1200 - 1330 MPa are cut using a slower cutter speed and we see that this has effectively reduced vibration levels and $||\mathbf{x}^{(4)}||_{6,1/N}$ values are similar to cuts with yield strengths lower than 900 MPa in the case of thin steels. Thus, although more shock-like vibrations occur with higher strength steels, we can say that with slower operating speed the cutter can still be used safely at least with moderately thin steels. With medium thickness steels the $||\mathbf{x}^{(4)}||_{6,1/N}$ values have a lot of variation.

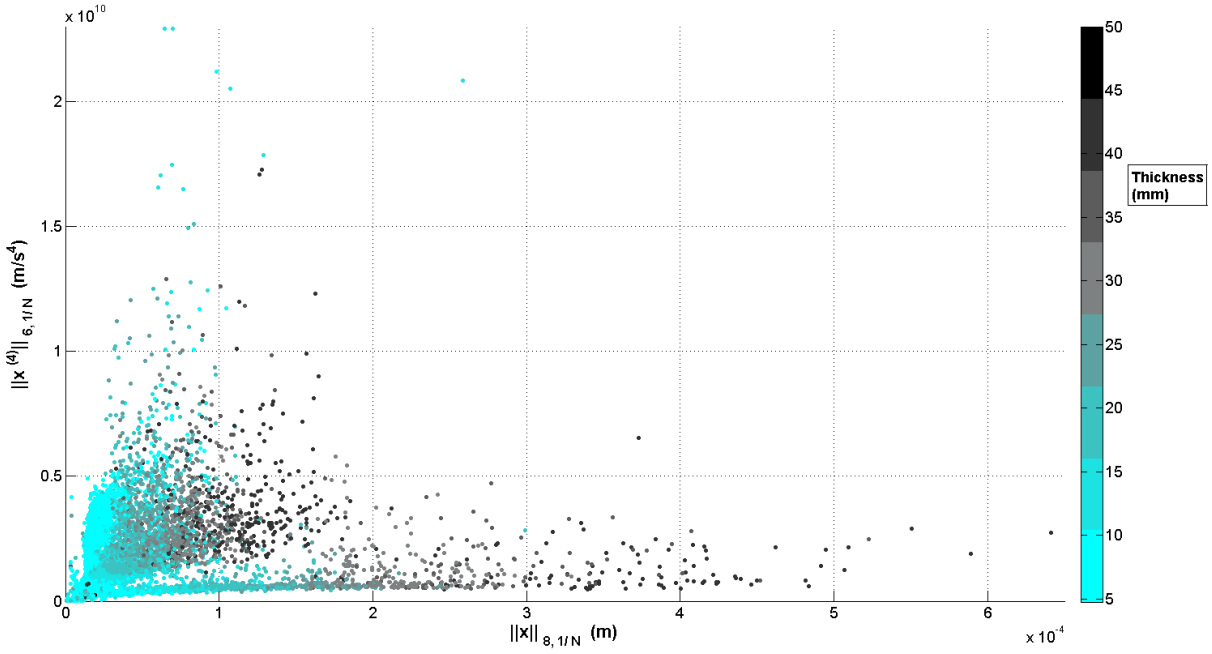

Fig. 8. 2D distribution of norms $||\mathbf{x}||_{8,1/N}$ and $||\mathbf{x}^{(4)}||_{6,1/N}$, color depicts steel thickness.

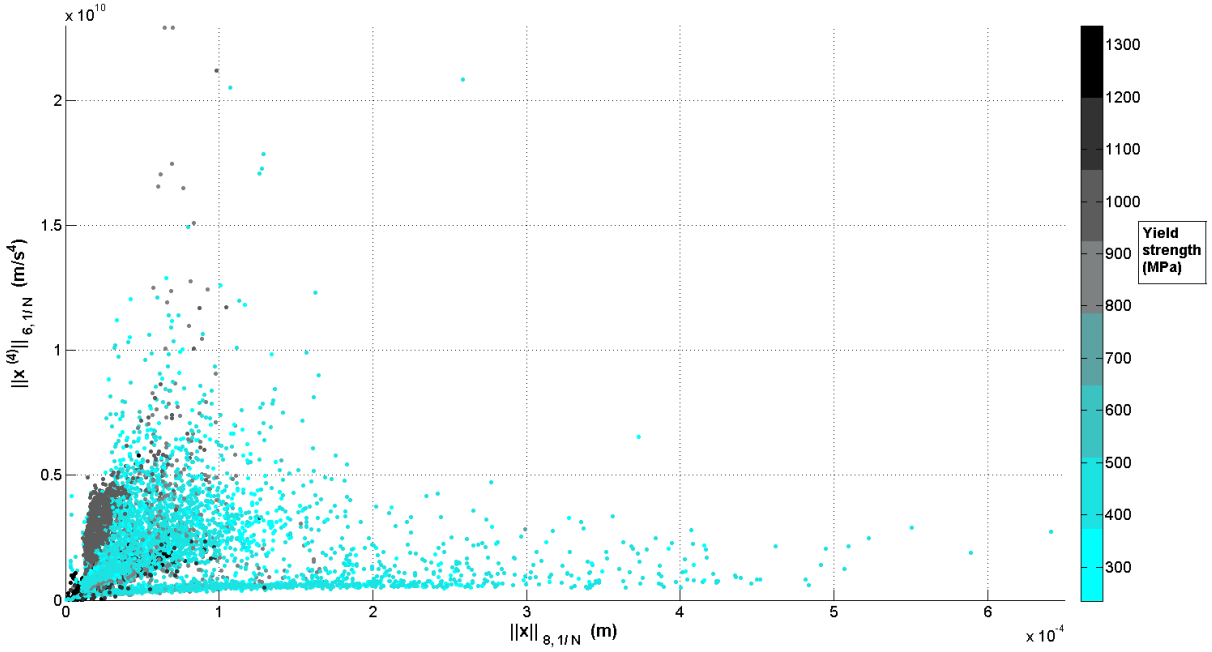

Fig. 9. 2D distribution of norms $||\mathbf{x}||_{8,1/N}$ and $||\mathbf{x}^{(4)}||_{6,1/N}$, color depicts yield strength of steel.

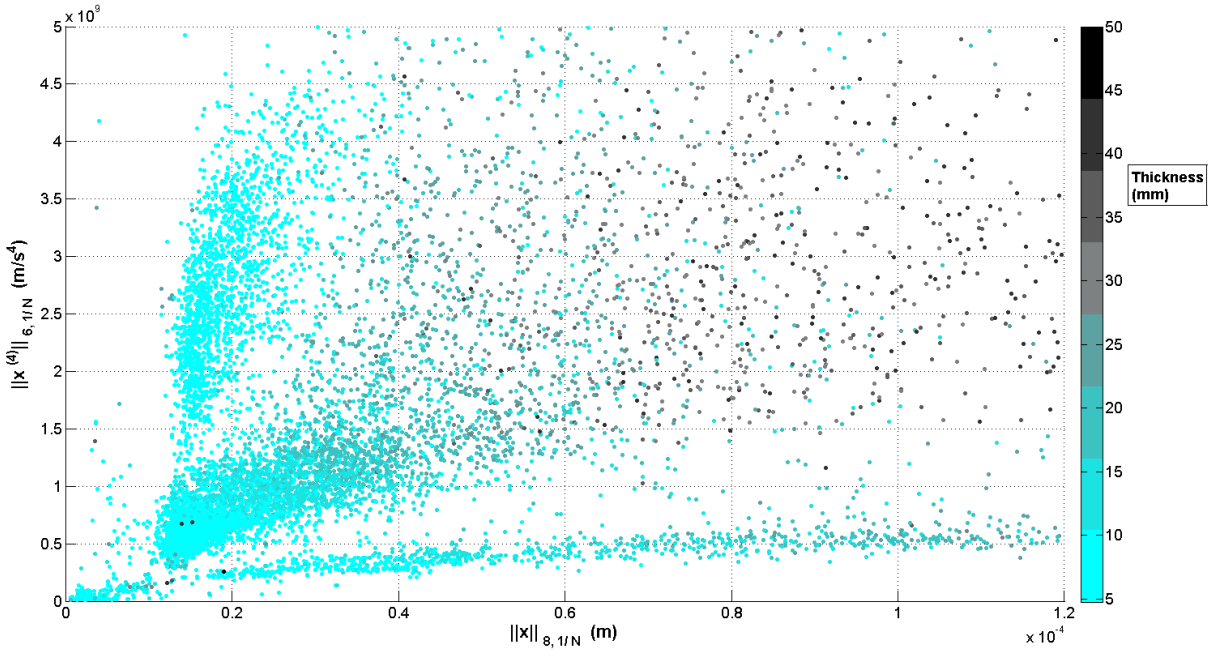

Fig. 10. Close up of Figure 8.

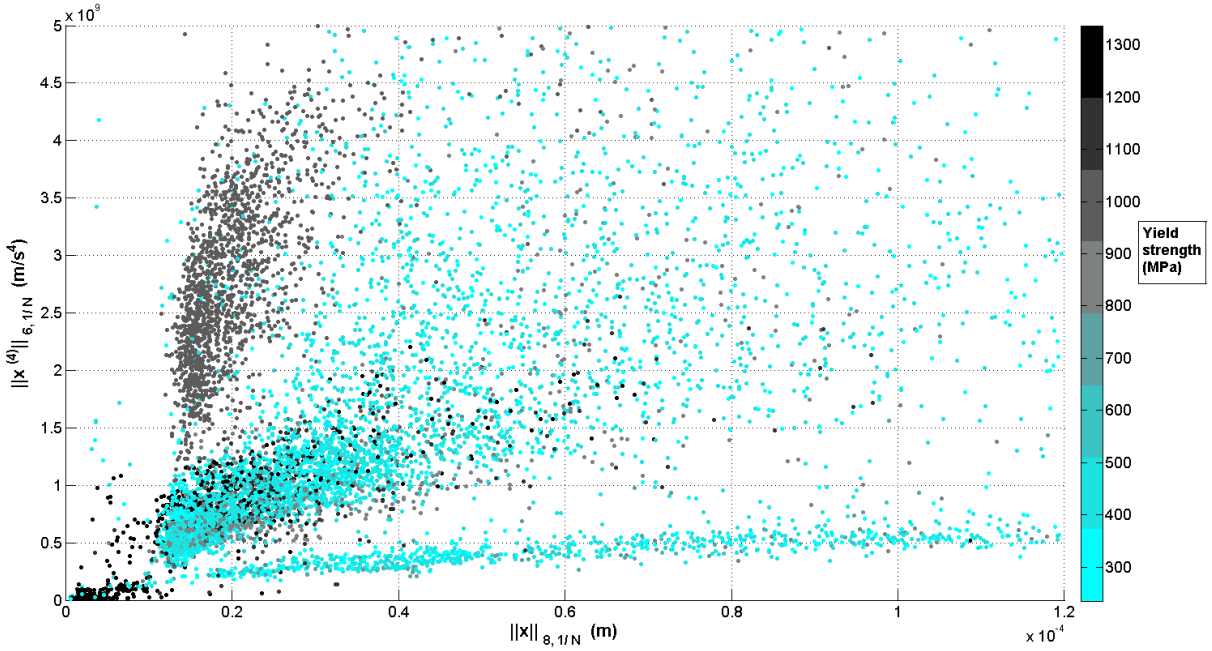

Fig. 11. Close up of Figure 9.

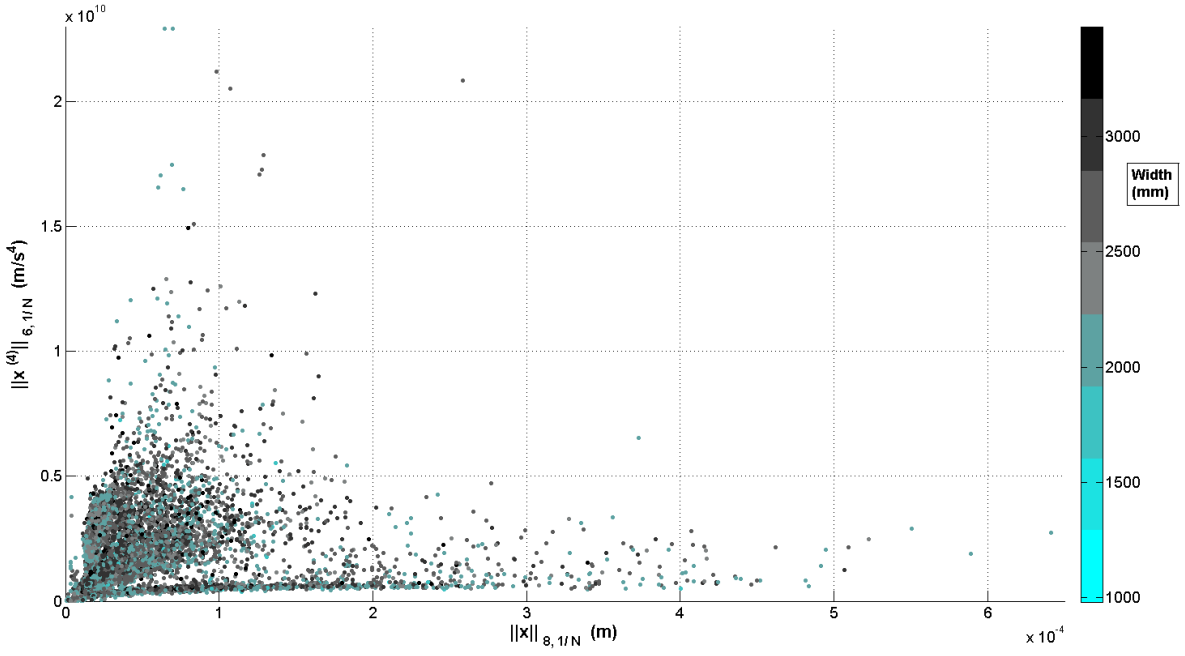

Fig. 12. 2D distribution of norms $||\mathbf{x}||_{8,1/N}$ and $||\mathbf{x}^{(4)}||_{6,1/N}$, color depicts steel width.

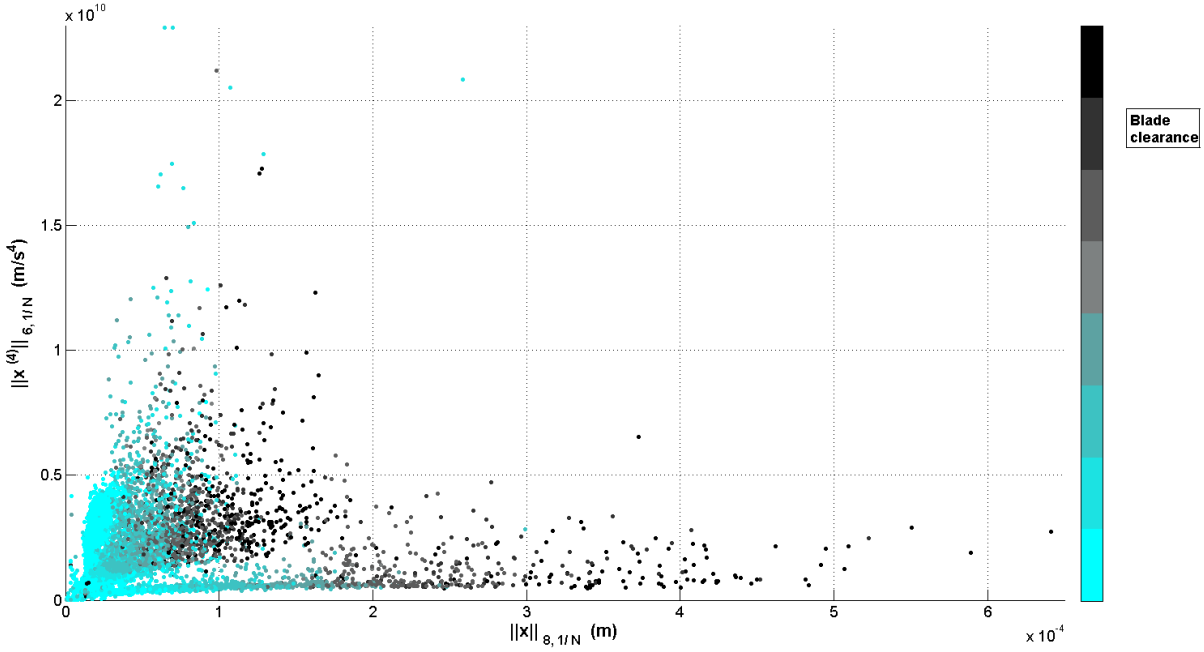

Fig. 13. 2D distribution of norms $||\mathbf{x}||_{8,1/N}$ and $||\mathbf{x}^{(4)}||_{6,1/N}$, color depicts cutter blade clearance.

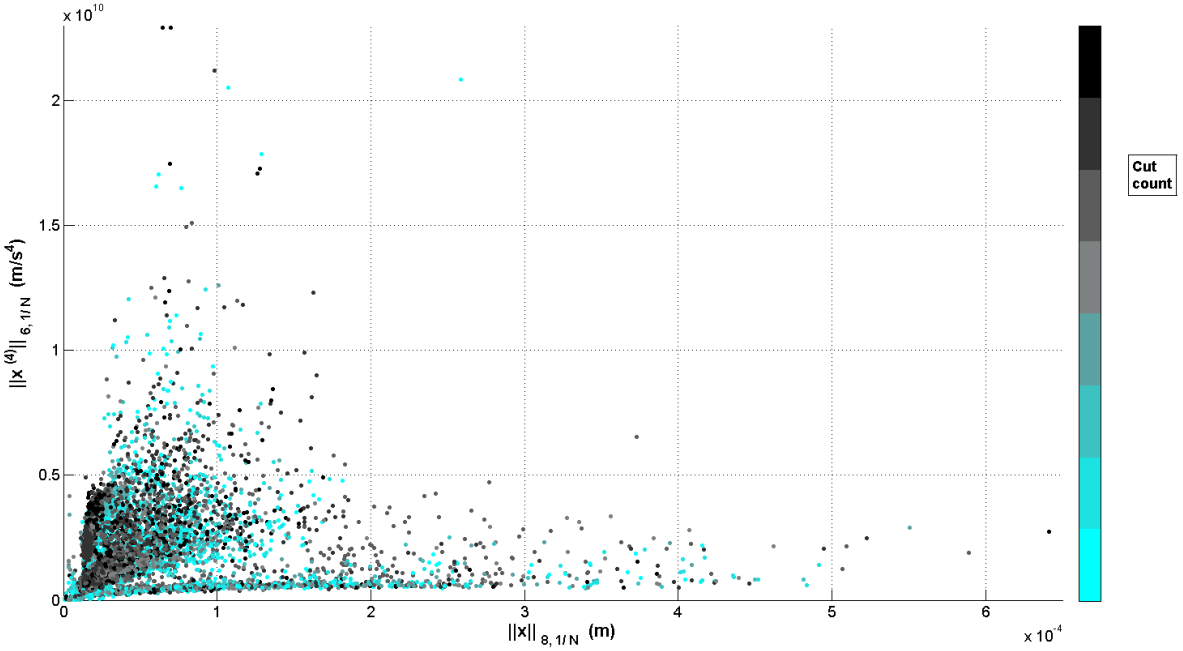

Fig. 14. 2D distribution of norms $||\mathbf{x}||_{8,1/N}$ and $||\mathbf{x}^{(4)}||_{6,1/N}$, color depicts cut count after blade replacement.

REFERENCES

Bullen, P. S. (2003). Handbook of Means and Their Inequalities. 2nd ed. Kluwer Academic Publishers, Dordrecht, 537 p.

Fourier, J. (1822). Théorie analytique de la chaleur. Firmin Didot, Paris, 637 p.

Karioja, K. and Lahdelma, S. (2015). Applying weighted $\bar{l}_p$-norms and MIT measurement indices in the stress evaluation of a steel cutter. The International Journal of Condition Monitoring, 5(1), 20–27.

Lahdelma, S. (1992). New vibration severity evaluation criteria for condition monitoring. In Finnish, University of Oulu, Research report No 85, 18 p.

Lahdelma, S. and Juuso, E. (2011). Signal processing and feature extraction by using real order derivatives and generalised norms. Part 1: Methodology. The International Journal of Condition Monitoring, 1(2), 46–53.

Lahdelma, S. and Kotila, V. (2005) Complex Derivative - A New Signal Processing Method. Kunnossapito, 19(4), 39–46.

Nissilä, J. Lahdelma, S. and Laurila, J. (2014). Condition monitoring of the front axle of a load haul dumper with real order derivatives and generalised norms. In 11th International Conference on Condition Monitoring and Machinery Failure Prevention Technologies, CM 2014 and MFPT 2014, Manchester, UK, June 2014, 20 p.

Samko, S. G. Kilbas, A. A. and Marichev, O. I. (1993). Fractional Integrals and Derivatives. Theory and Applications. Gordon and Breach, Amsterdam, 976 p.

Weyl, H. (1917). Bemerkungen zum Begriff des Differentialquotienten gebrochener Ordnung. Vierteljahrsschrift der Naturforschenden Gesellschaft in Zürich, 62(1-2), 296–302.